3D CSEM Forward Modelling: Testing Adaptive Mesh Refinement Approaches on an Ore Body Model

Paula Rulff[1], Thomas Kalscheuer[1], Laura Maria Buntin[1], Mehrdad Bastani[1,2]
[1]Dept. of Earth Sciences, Uppsala University, Sweden [2]Geological Survey of Sweden (SGU), Uppsala, Sweden
paula.rulff@geo.uu.se

SMARTEXPLORATION
new ways to explore the subsurface

UPPSALA UNIVERSITET

Key Features of the Modelling Code

- **3D controlled-source electromagnetic** (CSEM) modelling in **frequency domain**
- Using **unstructured tetrahedral meshes** of **finite-elements**
- First order **Nédélec basis functions** - vector edge interpolation functions [1]
- **Dirichlet boundary conditions**
- Model parameters: **electric resistivity** and **magnetic permeability**
- Calculation of the electric fields in an edge-based manner
- **Curl-Curl-Equation** for the electric field (**E**) with time dependency of $e^{i\omega t}$:

$$\nabla \times \frac{1}{\mu}\nabla \times \mathbf{E} + i\omega\frac{1}{\rho}\mathbf{E} = -i\omega \mathbf{J}_{source} \qquad (1)$$

- Latest addition: **goal-oriented adaptive mesh refinement**
- Planned to be incorporated in the inversion framework EMILIA [2] as a 3D module

Refinement Approach

Dual weighting

- Dual problem formulation for CSEM modelling based on Ren, 2013 [3]
- **New**: artificial influence source currents $\mathbf{J}_r$ of amplitude r^3, where r is the source-receiver distance
- **Aim**: equal weighting of the receivers in the goal-oriented refinement

Relative error estimator

- Obtained from primary and dual solution
- Based on residuals r, face jumps in normal current density $J^{\tilde{n}}$ and face jumps in tangential magnetic field $H^{\tilde{n}\times}$ (Ren, 2013 [3], Grayver & Kolev, 2015 [4])
- **New**: weighting based on local field amplitudes
- **Aim**: obtain an error estimator relative to the amplitude of the local field generated by a controlled source

Refinement strategy

- Elements whose error estimators exceed a certain threshold are refined
- Evaluation of the refinement using an *average relative global error estimate* η_G & and an *average relative error estimate at the receivers* η_R
- Low-quality (high q-value) starting mesh with few degrees of freedom
- Successive & problem-specific increase of the mesh quality during the refinement procedure

Refinement Validation

Model:

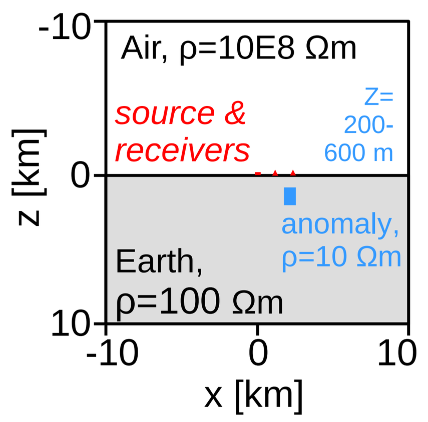

Figure 1: A vertical cut at y= 0 km through the modelling domain. The model contains an electric dipole source in the center, two inline receivers and a conductive block anomaly.

starting mesh		refined mesh	
14799 dof	12613 ele	33381 dof	28582 ele
modelling parameters		**ref. termination criteria**	
frequencies	1 - 100 Hz	max. dof	200 000
refinement frequency	100 Hz	max. iterations	100
mesh quality factor	1.5	desired accuracy	0.01

Refinement:

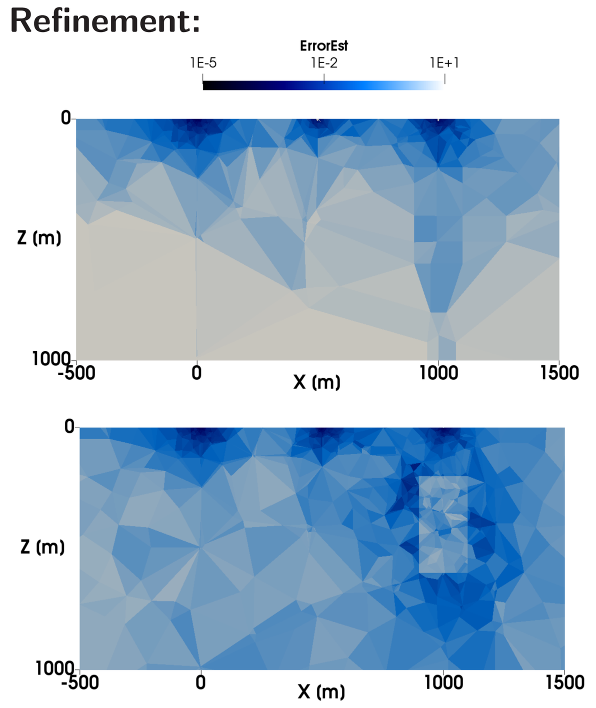

Figure 2: Initial and final elemental error estimators are shown at a vertical slice at $y = 0$ km through the centre region around the source and receiver set-up. The color scale is valid for both figures.

Improved result after refinement:

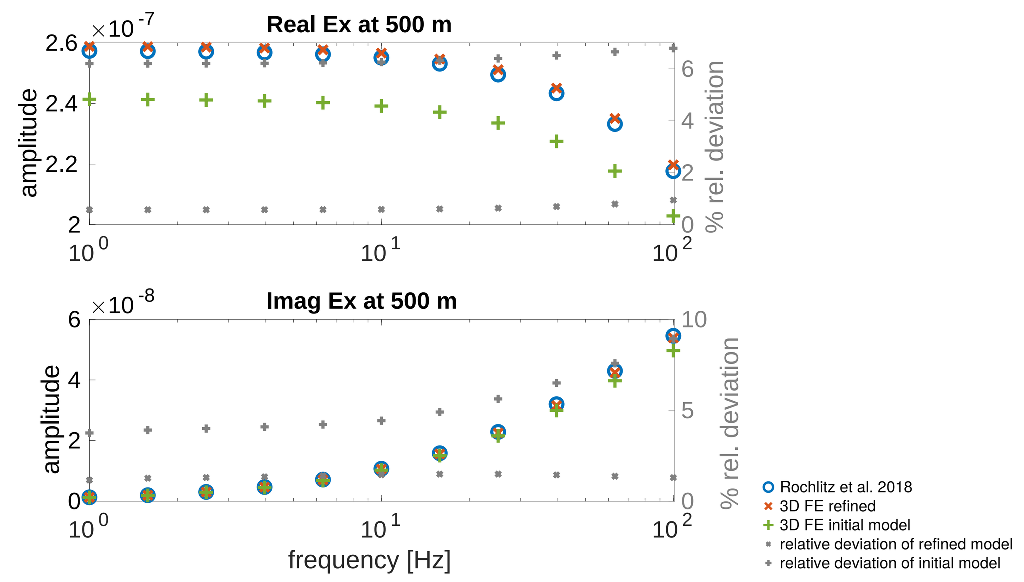

Figure 3: E_x component over frequency at the receiver at 500 m distance to the source midpoint. Shown is a reference solution calculated with custEM [6], our FEM solution on the initial mesh and on the final mesh. The relative deviations of the approximated solutions to the reference is shown in grey. For both imaginary and real parts of the depicted component, we observe a **clear improvement of our FEM solution after the refinement.**

Ore Body Model

Model:

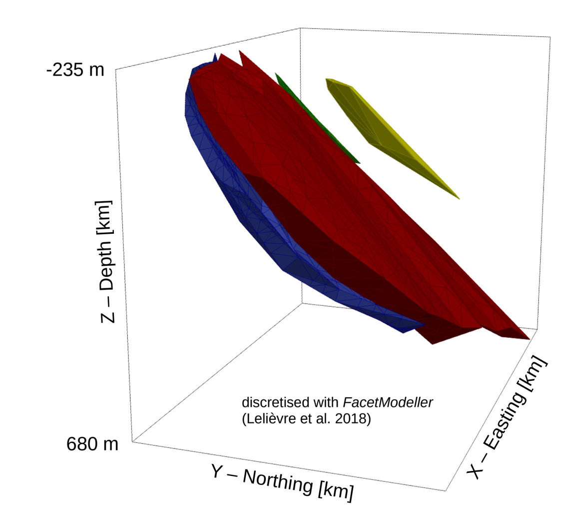

Figure 6: Shape of the orebodies obtained by borehole data [8] discretised with finite elements using tetgen [5] and FacetModeller [7].

Model dimensions: $60 \times 60 \times 60\ km^3$
Degrees of freedom: ca. 1 Mio.
Hostrock: $\rho = 10000\ \Omega m$, $\mu_r = 1.0$
Ore bodies: $\rho = 10/100/1000\ \Omega m$, $\mu_r = 1.3$
Source: extended HED x & y-polarisation, $10\ A$
Receivers: distributed around the ore body location
Frequencies : $100\ Hz$ - $10\ kHz$

Refinement without volume constraints:

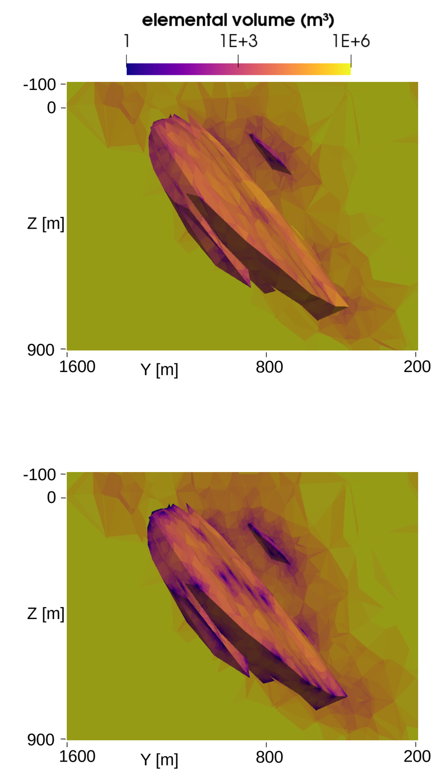

Figure 7: Distribution of elemental volume for the initial mesh (top) and the medium sized mesh after refinement with $q = 1.6$ (bottom) without imposing volume constrains within the ore bodies. The view plane is a vertical slice through the domain at $x = 2230$ m.

Refining a model with detailed subsurface anomalies as the ore bodies is challenging.

As a result of an internal setting of the mesh generator, that ensures to fulfill certain tolerance thresholds regarding the coplanarity of vertices, **excessive refinement takes place at the surface of the anomaly** (Figure 7) .

We thus enforce small elements in the ore bodies in the initial mesh (Figure 8 top) and run 10 refinement steps, each with a q-value increasing by 0.05 and an accordingly chosen vertex coplanarity tolerance value.

This adds a global refinement component to the goal-oriented one and results in less refinement steps and a reasonable refinement behaviour: **The region around the source, the receivers and the anomaly is refined (Figure 8 bottom)**.

Refinement with volume constraints:

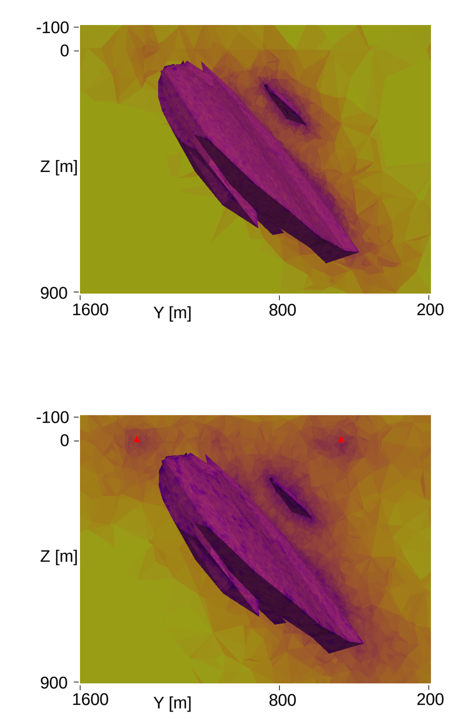

Figure 8: Distribution of elemental volume for the initial mesh (top) and the medium sized mesh after refinement with $q = 1.6$ (bottom) imposing volume constraints within the ore bodies. The view plane is a vertical slice through the domain at $x = 2230$ m. The color scale is the same as in Figure 7. Receiver locations are marked with red triangles.

References

[1] J. Jin. The Finite Element Method in Electromagnetics. Wiley-IEE Press, 3th edition, 2014.
[2] T. Kalscheuer, M. d. l. A. Garcia Juanatey, N. Meqbel, L. B. Pedersen. Non-linear model error and resolution properties from two-dimensional single and joint inversions of direct current resistivity and radiomagnetotelluric data. Geophys. J. Int., 182(3):1174-1188, 2010.
[3] Z. Ren, T. Kalscheuer, S. Greenhalgh, & H. Maurer. A goal-oriented adaptive finite-element approach for plane wave 3-D electromagnetic modelling. Geophysical Journal International, 194, 700–718, Oxford University Press, 2013.
[4] A.V. Grayver & T.V. Kolev. Large-scale 3D geoelectromagnetic modeling using parallel adaptive high-order finite element method. Geophysics, 80, E227–E291, Society of Exploration Geophysicists, 2015.
[5] Hang Si. TetGen, a Delaunay-Based Quality Tetrahedral Mesh Generator. ACM Trans. on Mathematical Software. 41(2), Article 11 (February 2015), 36 pages, 2015.
[6] R. Rochlitz, N. Skibbe, T. Günther. custEM: customizable finite element simulation of complex controlled-source electromagnetic data. Geophysics, 84(2), F17–F33, 2018.
[7] P.G. Lelièvre, A.E. Carter-McAuslan, M.W. Dunham, D.J. Jones, M. Nalepa, C.L. Squires, C.J. Tycholiz, M.A. Vallée. & C.G. Farquharson. FacetModeller: Software for manual creation, manipulation and analysis of 3D surface-based models, 2018.

[8] Provided by Nordic Iron Ore.

EGU General Assembly #EGU20

Permeable Subsurface

Model:

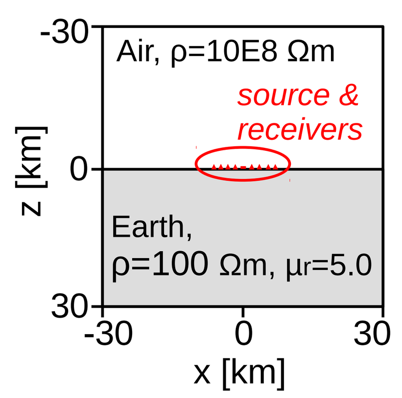

Figure 4: A vertical cut at y= 0 km through the modelling domain. The model contains an electric dipole source in the center and 146 inline receivers. The subsurface is a conductive and permeable half space.

To find the **optimal error estimator** for models with **contrasts in electric resistivity and magnetic permeability**, we run a few refinement steps for a homogeneous half space model discretised with a low quality factor of 1.6 and investigate the behaviour of the two average error estimators η_G and η_R for three cases: the approach based on residuals, face jumps in normal current density and face jumps in tangential magnetic field (*rJH*), the error estimation approach based on only face jumps in current density (J) and the one based on residuals and face jumps in current density (rJ).

The *rJH* approach causes both average error estimators to decrease most continuously and results in the lowest average error estimates after 12 refinement steps.

Behaviour of error estimates:

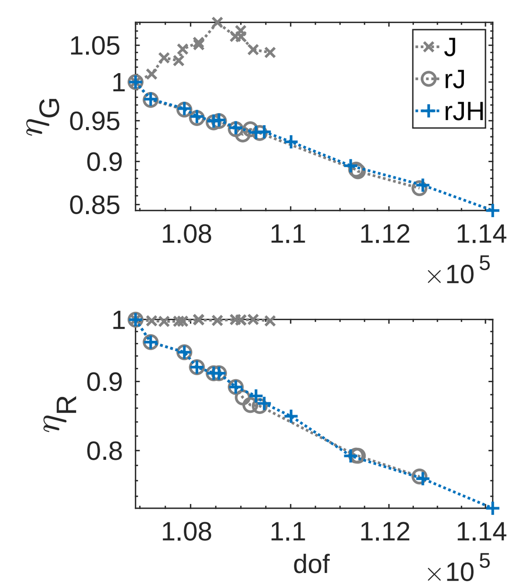

Figure 5: Average relative error estimates over degrees of freedom during a refinement procedure of 12 steps with a constant quality factor. Top panel: average relative *global* error estimate η_G. Bottom panel: average relative error estimate *at receivers* η_R.

Detectability

Figure 9: Amplitudes and phases of the strongest field components at a receiver above the ore bodies for the homogeneous half space model and three different ore body resistivity scenarios.

Detectability: anomalies are numerically detectable with the planned measurement setup. Ambient noise amplitudes at the CSEM frequencies in the measurement area are needed to make meaningful statements about the detectability with real measurements.

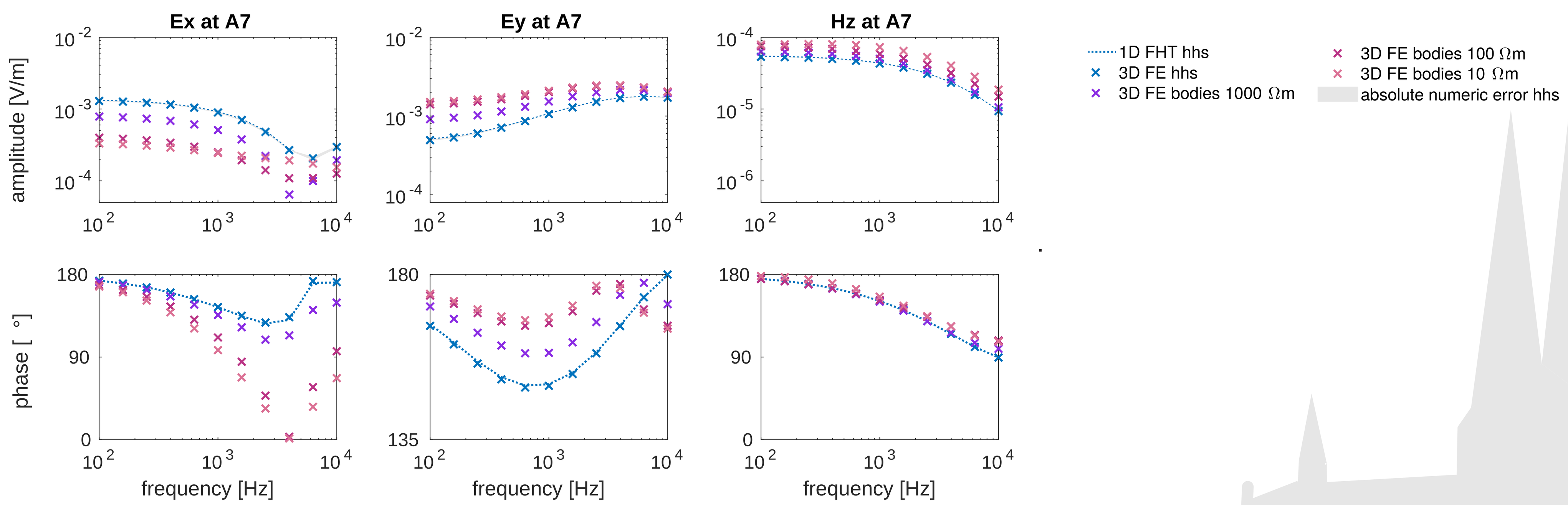

We thank Raphael Rochlitz for providing the custEM results.

This work is funded by the Smart Exploration project. Smart Exploration has received funding from the European Union's Horizon 2020 research and innovation programme under grant agreement No. 775971.